Electronic Supplementary Information

Viologen-functionalized metal-organic framework for efficient CO_2 photoreduction reaction

Tong Wang,[a] Lei Zhang,[b] Jiang Liu*[,a,b] Xiao-Xin Li,[a,c] Lin Yuan,[a] Shun-Li Li,[b] and Ya-Qian Lan*[,a,b]

[a] *Jiangsu Collaborative Innovation Centre of Biomedical Functional Materials, Jiangsu Key Laboratory of New Power Batteries, School of Chemistry and Materials Science, Nanjing Normal University, Nanjing 210023, P. R. China*

[b] *School of Chemistry, South China Normal University, Guangzhou, 510006, P. R. China*

[c] *School of Chemistry and Chemical Engineering, Southeast University, Nanjing 211189, P. R. China*

E-mail: liuj@njnu.edu.cn; yqlan@m.scnu.edu.cn; yqlan@njnu.edu.cn

Homepage: http://www.yqlangroup.com

Materials.

All starting materials, reagents and solvents used in experiments except 1,1'−bis (2, 4−dinitrophenyl) − (4,4'−bipyridinium) dichloride were commercially available, high-grade purity materials and used without further purification. Titanium tetraisopropanolate ($Ti(O^iPr)_4$, 95%), 2−aminoterephthalic acid (BDC−NH_2) and 4,4'−bipyridine were purchased from Aladdin; triethanolamine (TEOA), acetonitrile (MeCN), methanol (MeOH) and 2, 4−dinitrochlorobenzene were purchased from Adamas-beta.

Instruments. The surface morphology of catalysts was collected using high resolution thermal field emission scanning electron microscope (SEM, JSM-7600 F) with an acceleration voltage of 10 kV. Powder X-ray diffraction (PXRD) spectra were recorded on a Rigaku SmartLab diffractometer equipped with graphite monochromatized Cu Kα radiation (λ = 1.54060 Å) at 40 kV and 200 mA. Thermogravimetric analysis (TGA) was performed on a Diamond DSC Pyris analyzer (Perkin-Elmer) at a heating rate of 10 °C / min from ambient temperature to 800 °C under the air atmosphere. Fourier transform Infrared (FTIR) spectrum using the KBr pellet was measured on a Brucker Tensor 27 in the range of 4000-400 cm^{-1}. X-ray photoelectron spectroscopy (XPS) were recorded using Escalab 250Xi instrument (Thermo Scientific) equipped with an Al Kα microfocused X-ray source. UV-vis diffuse reflectance spectroscopy was acquired on a Varian Cary 5000 UV-Vis spectrophotometer in the wavelength range of 250-800 nm. The photoproduced liquid products were analyzed by ion chromatography (DIONEX AS-DV, Thermo Scientific). The gases (CO, CH_4 and H_2) were detected and analyzed by GC (GC-7900, CEAULIGHT) equipped with a flame ionization detector (FID, TDX-01 packed column) and a thermal conductivity (TCD, TDX-01 packed column). The^{13}C Nuclear Magnetic Resonance (NMR) was carried out AVANCE III 400M spectrometer (Bruker). The electrochemical test was carried out with EC-Lab SP-150 workstation (Bio-Logic) and CHI 660E (CH Instruments). Electron paramagnetic resonance (EPR) spectra were obtained on a Bruker EMXPLUS at 298 K. The Magic-Angle Spinning Nuclear Magnetic Resonance Spectroscopy (MASNMR) spectrum were obtained on a Brooklyn 400. Photoluminescence (PL) spectra and time solve photoluminescence lifetime were recorded by Edinburgh FLS1000.

Synthesis method

The synthesis of MIL-125-NH_2.

MIL-125-NH_2 was synthesized by a modified method reported in literature.[1] Briefly, 2 − aminoterephthalic acid (BDC−NH_2) (0.73 g) and titanium tetraisopropanolate $Ti(O^iPr)_4$ (0.8 mL) were added into a solution containing DMF (40 mL) and dry MeOH (5 mL). The above mixture was stirred at room temperature for 30 min and was transferred to a 100 mL glass reactor, and heated at 120°C for 48 hours. After reaction, the yellow powder was collected by centrifugation. The obtained material was washed with DMF (3 × 50 mL), and then with MeOH (3× 50 mL), and dried overnight at 60 °C.

The synthesis of 1,1' −bis (2, 4−dinitrophenyl) − (4,4' −bipyridinium) dichloride.

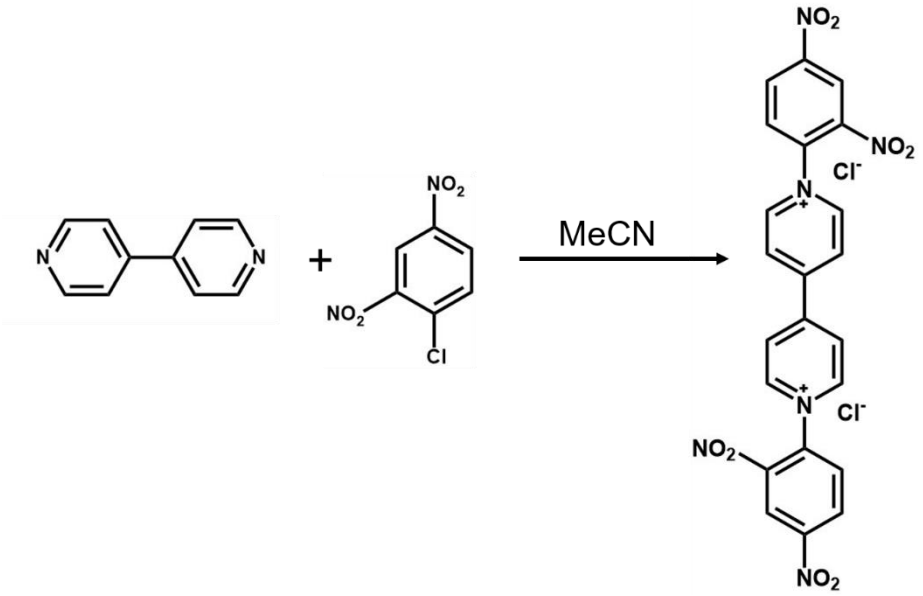

Synthesis method with reference to previous reports.[2] MeCN (70 mL) solution of 4,4'−bipyridine (3.6 g, 23 mmol) and 2, 4−dinitrochlorobenzene (16.5 g, 81 mmol) were heated at reflux for 72 hours. Filter the hot reaction mixture and reflux the filter cake with ethanol (300 mL). The precipitate was dried under vacuum and collected as white solid (6.0 g, 50%).

The synthesis of MIL-125-RV^{2+}.

MIL-125-RV^{2+} was synthesized with post-synthetic modification.[3, 4] 1,1'−bis (2, 4−dinitrophenyl) − (4,4'−bipyridinium) dichloride (1.0 g) and **MIL-125-NH_2** (0.5 g) were dispersed into a mixture of ethanol and water (v:v = 4:1, 50 mL). The mixture was heated under reflux and stirred for 24 h. At this stage the color of the suspension was changing from colorless to brown. Hot suspension was be filtered to prevent the precipitation of 2,4−dinitroaniline, and the brown solid was collected. To remove excess reactants, the obtained solid was washed with MeOH until the filtrate was colorless. Then the brown solid was dried under vacuum at 60 °C overnight. Finally, the pure **MIL-125-RV^{2+}** was obtained.

Photocatalytic CO_2 reduction test.

The crystals of **MIL-125-RV^{2+}** and **MIL-125-NH$_2$** were soaked in 20 mL of MeCN for 3 days replacing the solvent every 12 h and air-dried to be prepared. Photocatalytic reduction of CO_2 was performed in a 50 mL quartz reactor with as-prepared crystals. Photocatalysts (25 mg) were added into the mixed solution which contained MeCN (25 mL) and TEOA (5 mL) as electron donors. After degassing with high purity CO_2 to remove dissolved O_2 for 30 min, the reaction was performed under the irradiation of a 300 W Xe lamp with UV-cut to keep the wavelengths in the range from 420 to 800 nm. The reaction temperature was controlled at 303 K by using the cooling water circulation. In order to detect the content of gas-phase products produced by the reaction mixture, 500 μL of gas-product was extracted from the reactor with a syringe and injected into the gas chromatograph with an FID detector, using nitrogen as the carrier gas and reference gas. The liquid product ($HCOO^-$) is analyzed by ion chromatography. All photocatalytic reactions were repeated at least five times to ensure the accuracy of the experimental data.

Electrochemistry measurements.

All electrochemical measurements (transient photocurrent (TPC), the Mott–Schottky spots and electrochemical impedance spectra (EIS)) were carried out with a CHI 660E electrochemical workstation *via* a conventional three-electrode system in a 0.5 M Na_2SO_4 aqueous solution (pH = 6.8). The working electrode was ITO glass plates coated with a catalyst-slurry, the counter electrode was a platinum foil, and the reference electrode was a saturated Ag/AgCl electrode. The Mott-Schottky plots were measured over an alternating current (AC) frequency of 500 Hz, 1000 Hz and 1500 Hz. EIS measurements were recorded over a frequency range of 1000 kHz – 0.1 Hz with ac amplitude of 20 mV at 0 V.

Preparation of the working electrode: 2 mg photocatalysts were mixed with 990 μL ethanol and 10 μL Nafion D-520 dispersion solutions to generate a homogeneous slurry. Subsequently, 200 μL of slurry was transferred and coated on Indium-Tin Oxide conductive film glass (ITO glass, 1 cm×2 cm) then dried at room temperature.

In Situ Fourier transform infrared (FTIR).

In situ FTIR measurements were performed using a Nicolet iS50 Fourier transform spectrometer equipped with a MCT diffuse reflectance accessory at the Infrared Spectroscopy. Before measurement, the catalysts were purged with nitrogen at 120°C for 1 h. The catalysts were subsequently cooled down to room temperature. A background spectrum with a resolution of 4 cm^{-1} was obtained in a nitrogen stream at room temperature. During the in-situ characterization, the catalysts were exposed to pure CO_2 and is continuously introduced into the chamber. The in situ infrared spectra were collected under dark conditions or after a certain irradiation time.

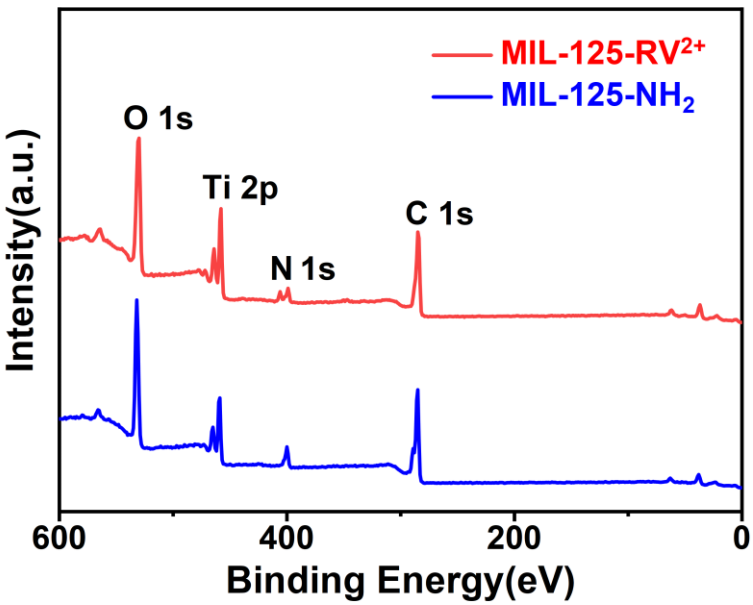

Fig. S1 The full-scan X-ray photoelectron spectroscopy (XPS) spectra of **MIL-125-NH$_2$** and **MIL-125-RV^{2+}**.

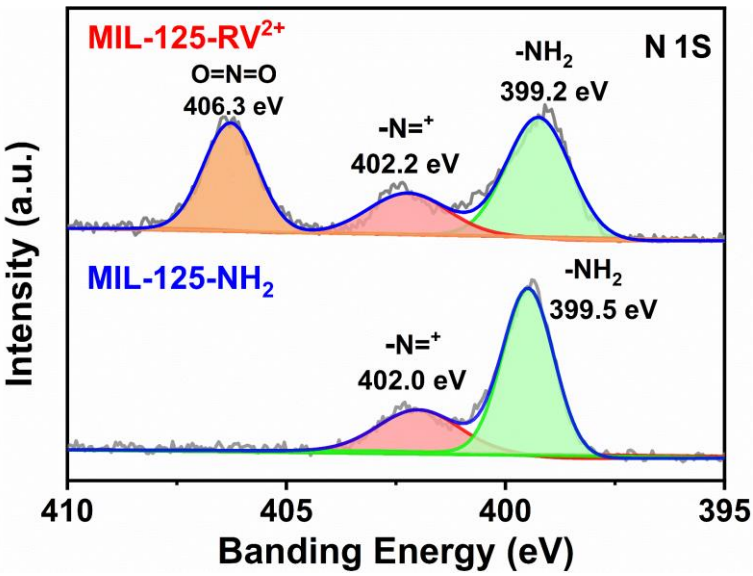

Fig. S2 The high-resolution N 1s XPS spectra of **MIL-125-NH$_2$** and **MIL-125-RV^{2+}**.[5]

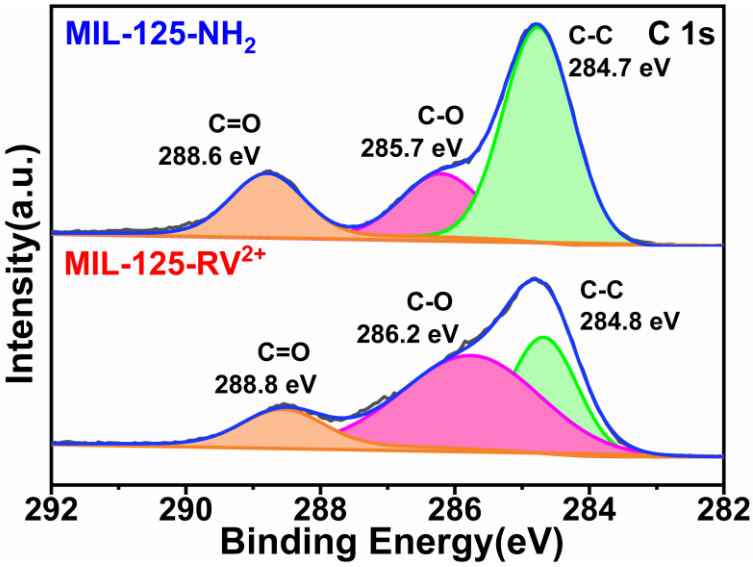

Fig. S3 The high-resolution C 1s XPS spectra of **MIL-125-NH$_2$** and **MIL-125-RV^{2+}**.[6]

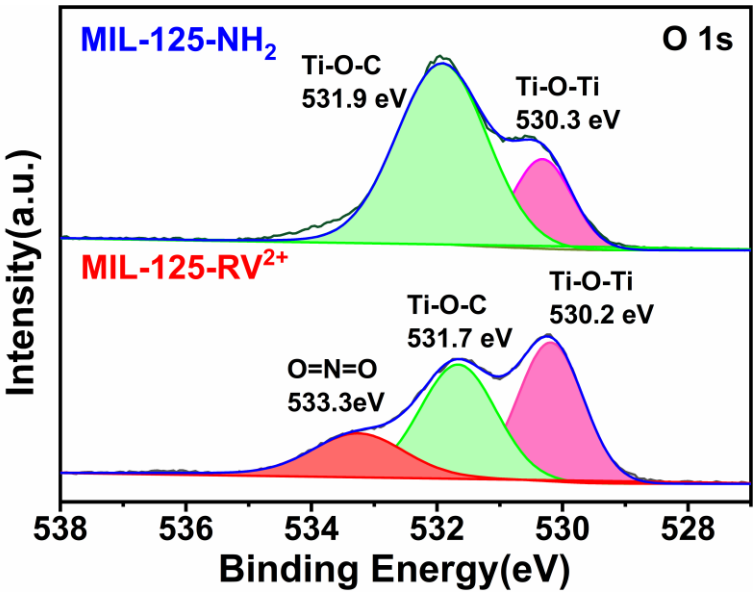

Fig. S4 The high-resolution O 1s XPS spectra of **MIL-125-NH$_2$** and **MIL-125-RV^{2+}**. A new peak appears at 533.3 eV, which indicates the presence of -NO_2.[7] The result is in agreement with the high-resolution N1s XPS spectra.

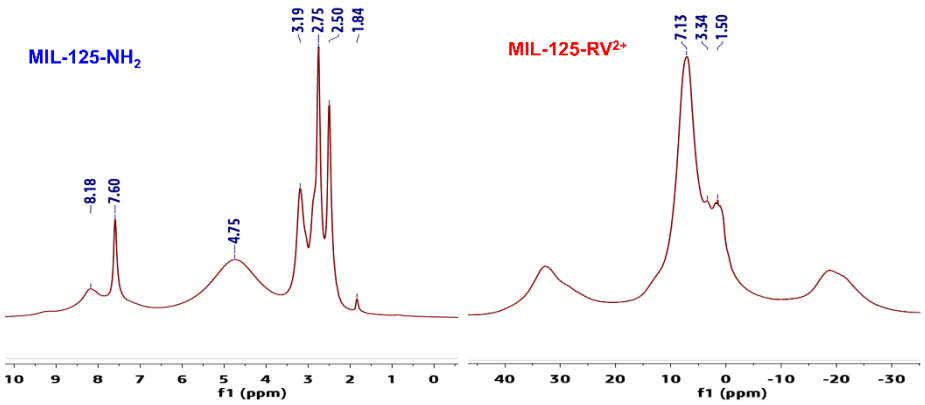

Fig. S5 The MASNMR spectra of **MIL-125-NH$_2$** and **MIL-125-RV^{2+}**. The ^{1}H MAS NMR spectra present the signal peak of -NH$_2$ (8.2ppm) disappeared. The result is consistent with the FTIR spectra.[8]

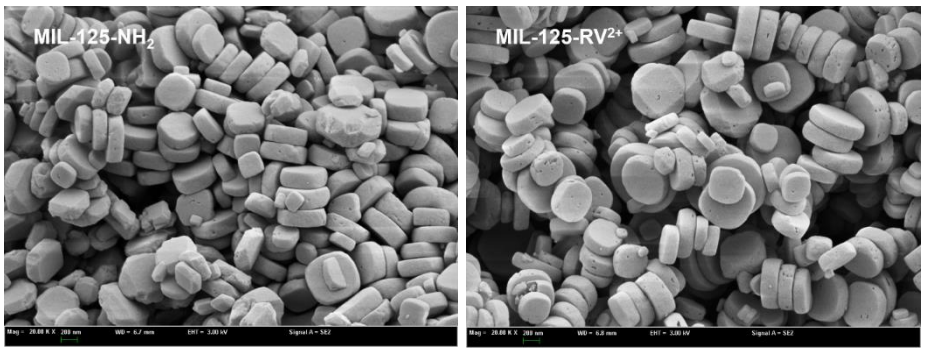

Fig. S6 Scanning electron microscopy (SEM) images of **MIL-125-NH$_2$** and **MIL-125-RV^{2+}**. The SEM images shows that the morphology of **MIL−125−RV^{2+}** was basically the same as the original **MIL−125−NH$_2$**,[9] which also confirms the integrity of the structure after modification.

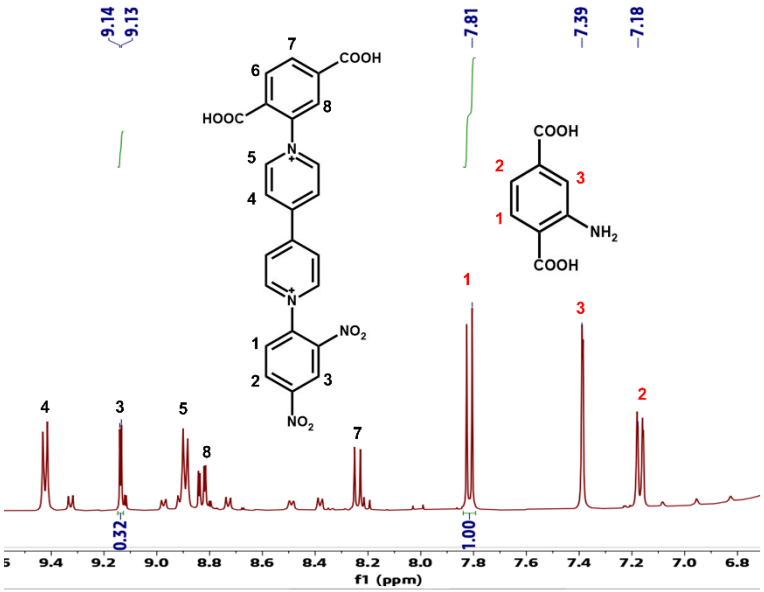

Fig. S7 ^{1}H NMR spectrum of the digested **MIL-125-RV^{2+}** in HF/DMSO-d_6.

Under extremely acidic conditions, the skeleton of MOFs is disrupted and the organic ligands are freed. The dominating manifestation of RV^{2+} on **MIL-125-RV^{2+}** is mono-linked. Therefore, the percentage of post-synthetic conversion was calculated using the relative integral area corresponding to the different aromatic protons on the two ligands shown in the figure.[10]

$$The\ conversion\ of\ RV^{2+} = \frac{0.32}{1.32} \times 100\% = 24.2\%$$

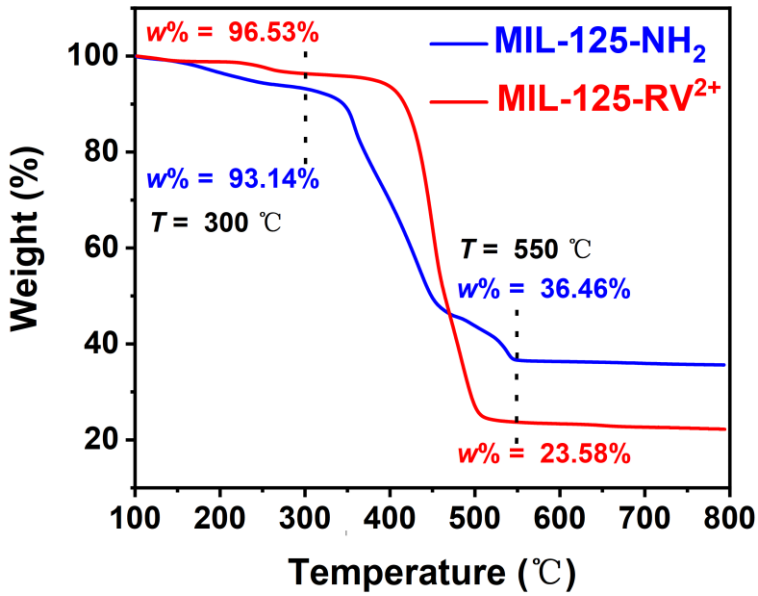

Fig. S8 Thermal gravimetrical analysis of **MIL-125-NH$_2$** and **MIL-125-RV^{2+}**.

The skeleton of **MIL-125-NH$_2$** and **MIL-125-RV^{2+}** was disrupted in the 300-550 °C range. The decomposition of organic ligands is usually in this temperature interval. Therefore, the percentage of post-synthetic modification was calculated from the weight loss in this temperature range.

$w_{\text{-NH2}}$ (300 °C) = 93.14%

$w_{\text{-NH2}}$ (550 °C) = 36.46%

w_{loss1} = 93.14% – 36.46% = 56.68%

$w_{\text{-RV2+}}$ (300 °C) = 96.53%

$w_{\text{-RV2+}}$ (550 °C) = 23.58%

w_{loss2} = 96.53% – 23.58% = 72.95%

$$The\ conversion\ of\ RV^{2+} = \frac{(w_{loss2} - w_{loss1})}{w_{loss1}} = 28.7\%$$

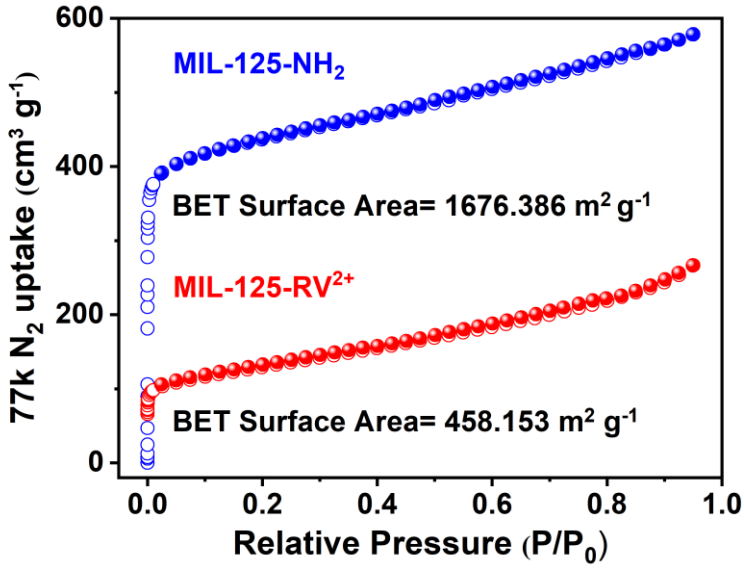

Fig. S9 N_2 sorption isotherms of **MIL−125−NH₂** and **MIL−125−RV^{2+}**.

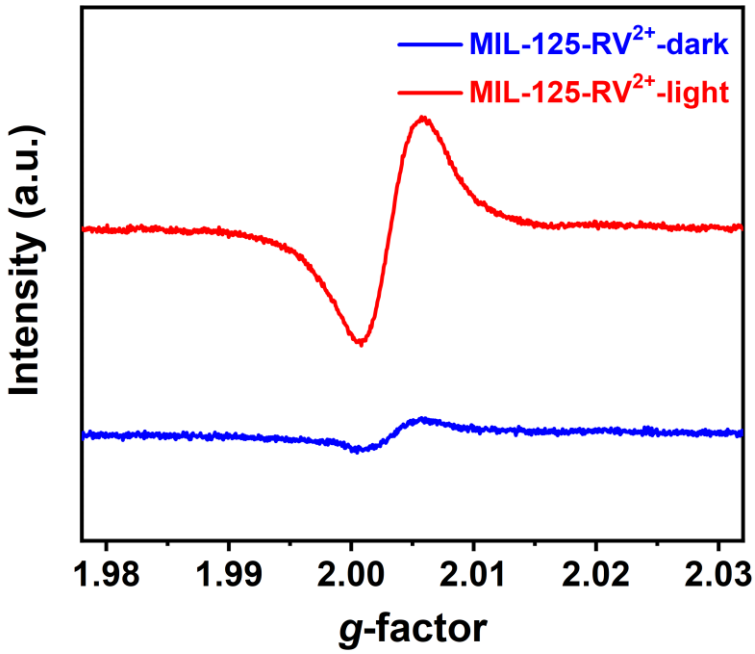

Fig. S10 EPR spectra of **MIL-125-RV^{2+}** before and after visible-light irradiation.

A weak free radical signal was detected by **MIL-125-RV^{2+}** in the dark.[11-13] Upon excitation by visible light, the intensity of this signal was significantly enhanced. This demonstrates that **MIL-125-RV^{2+}** underwent a rapid single electron transfer to form $RV^{\bullet+}$ upon visible light stimulation.

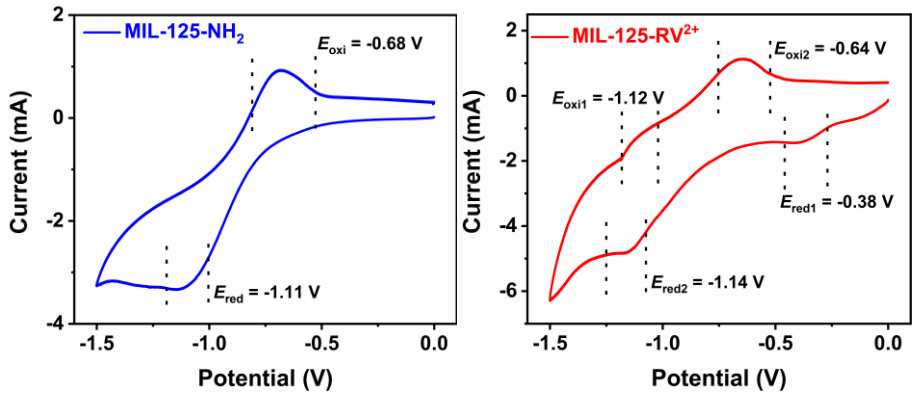

Fig. S11 Cyclic voltammogram of **MIL-125-NH$_2$** and **MIL-125-RV^{2+}** in MeCN containing 0.1 mol/L Bu_4NPF_6 at a scan rate of 100 mV/s.

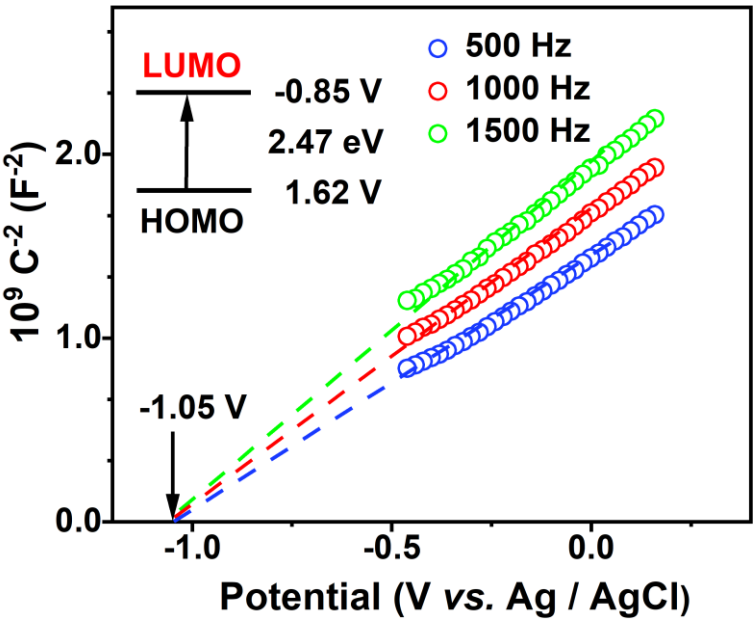

Fig. S12 Mott-Schottky plots for **MIL−125−NH$_2$** in 0.5 M Na_2SO_4 aqueous solution. Inset is the energy diagram of the HOMO and LUMO levels of **MIL−125−NH$_2$**.

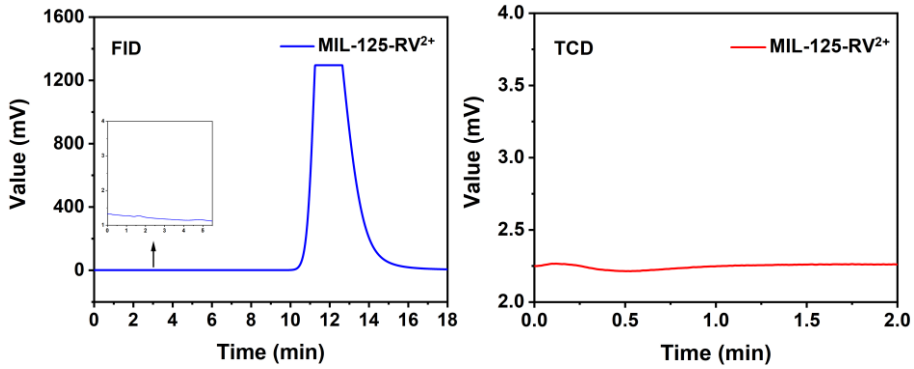

Fig. S13 GC analysis of the gas-phase reaction products for **MIL-125-RV^{2+}** by using the FID and TCD.

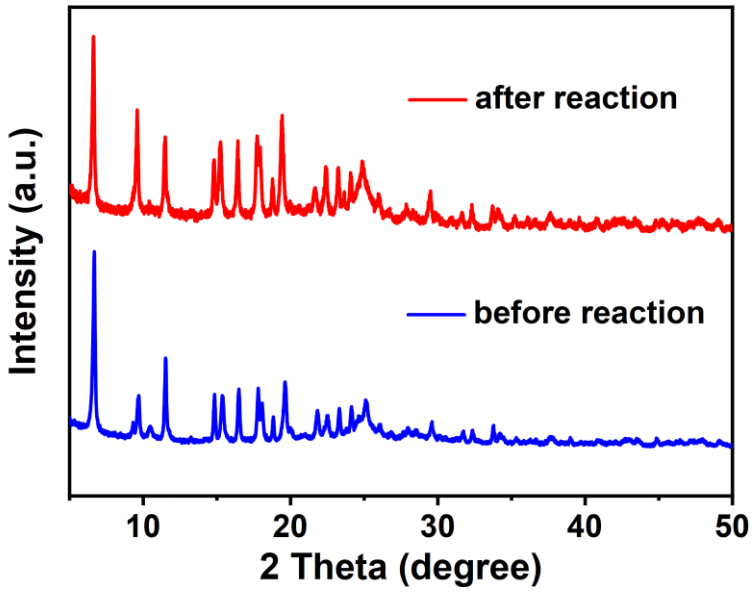

Fig. S14 PXRD patterns were performed before and after the photocatalytic reaction, confirming the structural robustness and heterogeneous photocatalytic nature of **MIL-125-RV^{2+}**.

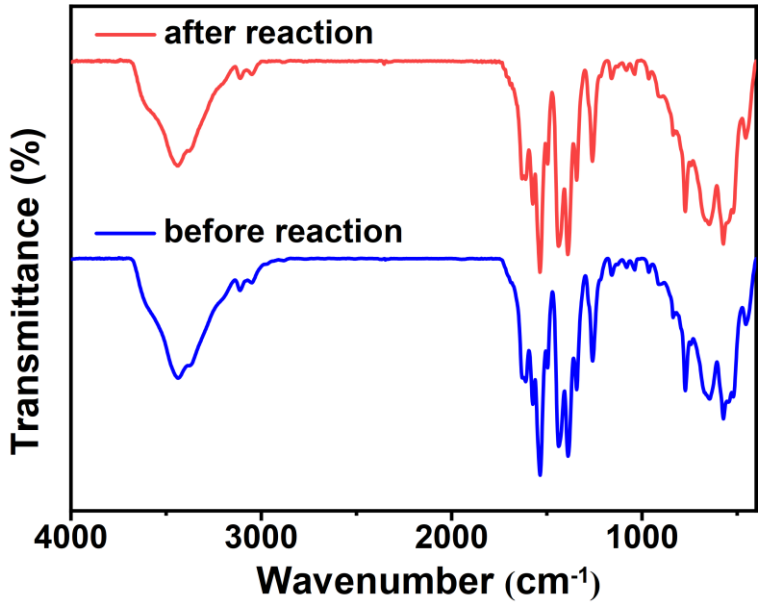

Fig. S15 FTIR spectra of **MIL-125-RV^{2+}** were performed before and after the photocatalytic reaction.

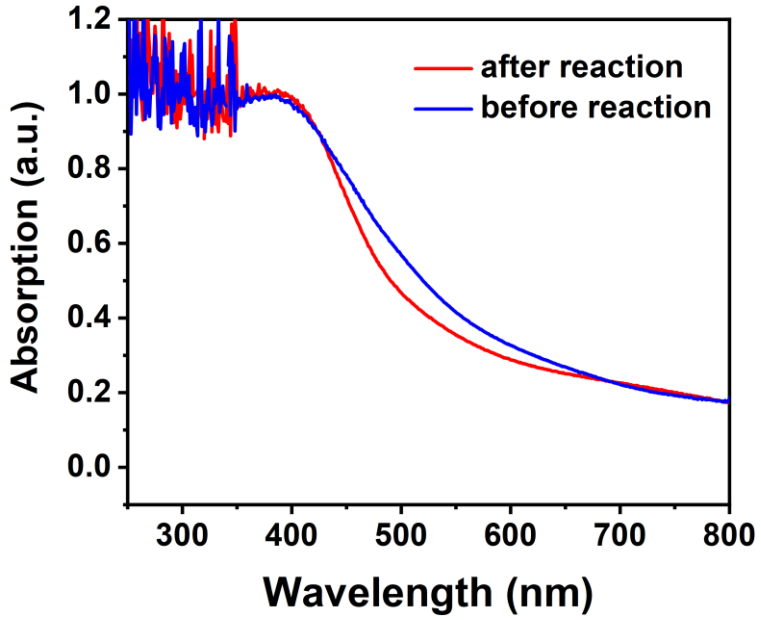

Fig. S16 UV−vis DRS spectra of **MIL-125-RV^{2+}** were performed before and after the photocatalytic reaction.

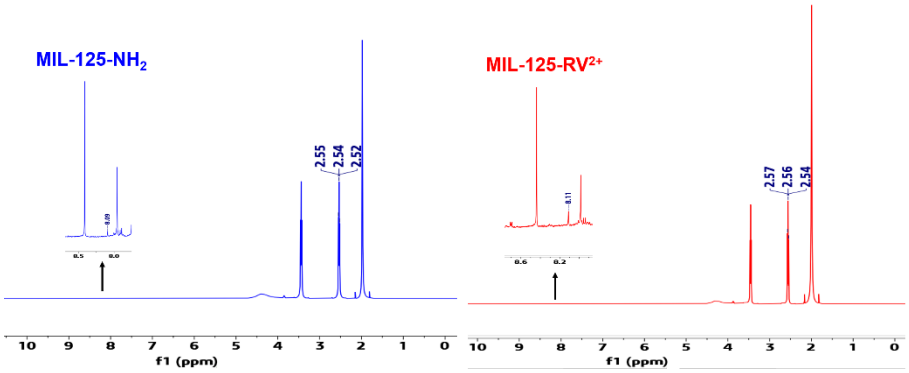

Fig. S17 ^{1}H NMR spectrum of solution obtained by photocatalytic CO_2RR of **MIL-125-NH$_2$** and **MIL-125-RV^{2+}**. The peaks at 8.11 ppm was attributable to $HCOO^{-}$.

Compared to **MIL−125−NH$_2$**, no additional peaks appeared in the ^{1}H NMR spectrum of the solution obtained after photocatalytic CO_2RR by **MIL−125−RV^{2+}**. It proves that the RV^{2+} molecules can be stabilized on the **MIL−125−NH$_2$** under the light irradiation.

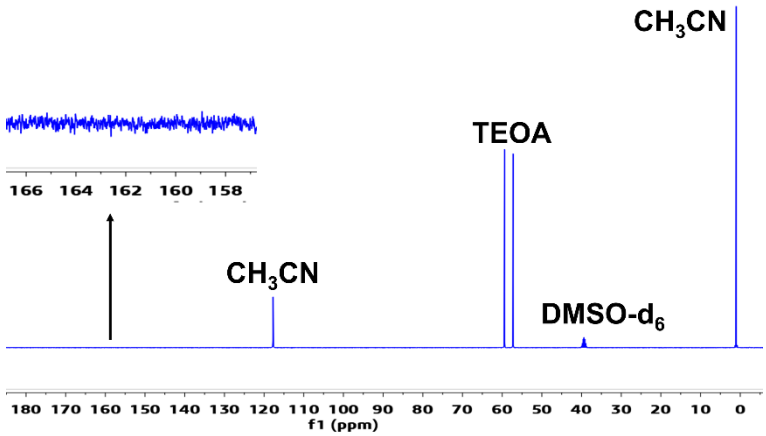

Fig. S18 The ^{13}C NMR spectrum of the product obtained by adding $^{12}CO_2$ into the reaction of **MIL-125-RV^{2+}**.

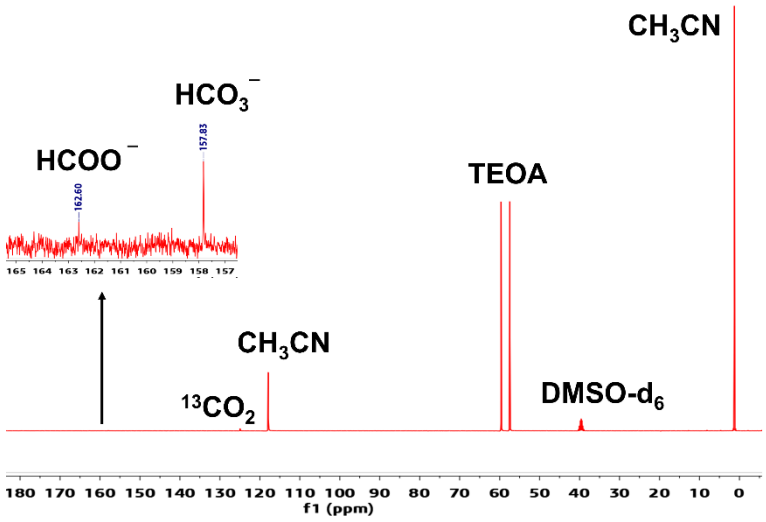

Fig. S19 The ^{13}C NMR spectrum of the product obtained by adding $^{13}CO_2$ into the reaction of **MIL-125-RV^{2+}**. The signal at 162.6 ppm was attributed to $HCOO^{-}$. (The standard ^{13}C NMR chemical shift of $HCOO^{-}$ is at 162.86 ppm).[14]

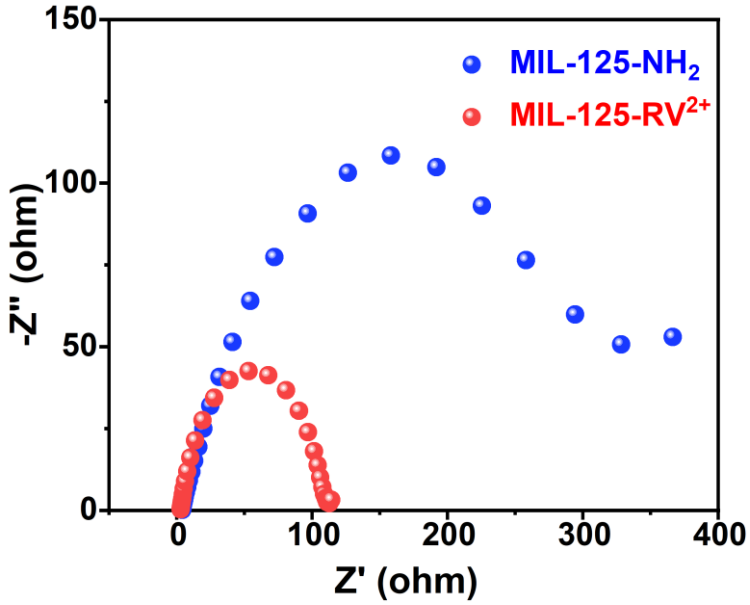

Fig. S20 Nyquist plots of **MIL-125-NH$_2$** and **MIL-125-RV^{2+}** over the frequency ranging from 1000 kHz to 0.1 Hz.

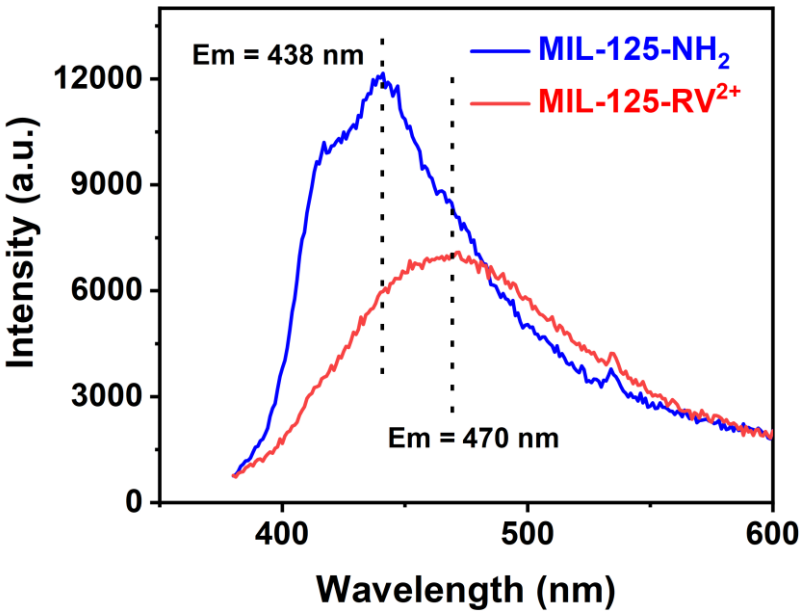

Fig. S21 PL spectra of **MIL-125-NH$_2$** and **MIL-125-RV^{2+}** under an excitation light of 365 nm.

It can be seen from the PL spectra that the viologen functionalized **MIL-125-RV^{2+}** indicate relatively weaker PL intensity compared to **MIL-125-NH$_2$**. This result reveals that the introduction of the RV^{2+} ligands on the **MIL-125-RV^{2+}** can effectively enhance the separation of electrons and holes within the molecule.[15, 16]

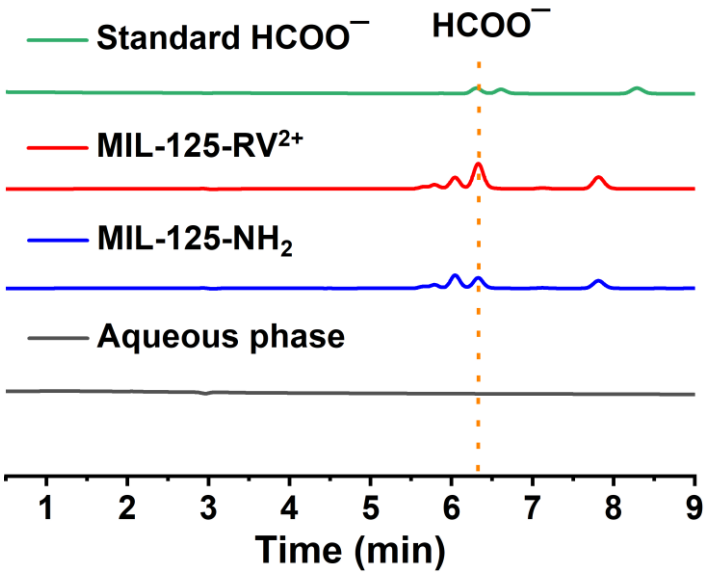

Fig. S22 Analysis of the liquid reaction products generated in photocatalytic system by ion chromatography.

Fig. S23 The photograph of photocatalytic reactor.

The AQE measurement:

The apparent quantum efficiency (AQE) for $HCOO^-$ evolution was measured using monochromatic visible light (420/450/500 nm). Depending on the amounts of $HCOO^-$ produced by the photocatalytic reaction in an average of one hour, and the AQE was calculated as follow:

$$AQE = \frac{(2 \times the\ number of\ HCOO^-) molecules\ produced}{the\ number\ of\ incident\ photons} \times 100\%$$

$$AQE = \frac{2 \times M \times N_A \times h \times c}{S \times P \times T \times \lambda} \times 100\%$$

M = yield of $HCOO^-$ (mol);
N_A (Avogadro constant) = 6.02×10^{23} mol^{-1};
h (Planck constant) = 6.626×10^{-34} J·s;
c (Speed of light) = 3 × 108 m/s;
S = Irradiation area (cm^2) = 7.06 cm^2;
P = the intensity of irradiation light (W / cm^2) = 55.4 mW / cm^2 (420 nm) or 59.7 mW / cm^2 (450 nm) or 60.8 mW / cm^2 (500 nm);
T = the photoreaction time (s) = 10 × 3600 = 36000 s;
λ = the wavelength of the monochromatic light (nm) = 420×10^{-9} m / 450×10^{-9} m / 500×10^{-9} m.

Table S1 Yield of $HCOO^-$ evolution with different monochromatic light (420/450/500 nm) on **MIL-125-NH_2 and MIL-125-RV^{2+}**.

Monochromatic light (λ)	420 nm	450 nm	500 nm
MIL-125-NH_2 ($HCOO^-$, μmol)	6.35	4.72	2.55
MIL-125-RV^{2+} ($HCOO^-$, μmol)	8.46	6.82	3.43

Table S2 Apparent quantum efficiency (AQE) of $HCOO^-$ evolution was measured with different monochromatic lights (420/450/500 nm) on **MIL-125-NH_2 and MIL-125-RV^{2+}**.

Monochromatic light (λ)	420 nm	450 nm	500 nm
AQE (MIL-125-NH_2)	0.027	0.019	0.010
AQE (MIL-125-RV^{2+})	0.034	0.028	0.014

The results of AQE data indicate that **MIL-125-NH_2** and **MIL-125-RV^{2+}** achieve the highest apparent quantum yield when irradiated with monochromatic light with a wavelength of 420 nm, and the AQE of **MIL-125-RV^{2+}** is much higher than of **MIL-125-NH_2**. It further confirms that the photocatalytic activity of **MIL-125-RV^{2+}** under visible-light irradiation far exceeds that of **MIL-125-NH_2**.[17]

Table S3 Comparative experiments under different conditions for the photocatalytic CO_2RR of **MIL-125-RV^{2+}**.

Photocatalyst	Atmosphere	Light Source	$HCOO^-$ (μmol)	H_2 (μmol)
MIL-125-RV^{2+}	CO_2	420-800	12.13	n.d.
MIL-125-RV^{2+}	Ar	420-800	n.d.	n.d.
MIL-125-RV^{2+}	CO_2	dark	n.d.	n.d.
no catalyst	CO_2	420-800	n.d.	n.d.
MIL-125-NH$_2$	CO_2	420-800	7.31	n.d.
MIL-125-NH$_2$+RV^{2+}	CO_2	420-800	--	--

Note: The physical mixture of **MIL-125-NH$_2$** (19 mg) and RV^{2+} molecules (6 mg) was applied to CO_2RR. But RV^{2+} molecules dissolved in the solution of acetonitrile and TEOA.

Table S4 The research of photocatalytic reaction conditions for **MIL-125-RV^{2+}**.

Entry	$HCOO^-$ (μmol)	CO (μmol)	CH_4 (μmol)	H_2 (μmol)	Selectivity for $HCOO^-$ (%)
1[a]	12.13	n.d.	n.d.	n.d.	100
2[b]	8.68	0.23	n.d.	1.72	83
3[c]	2.12	n.d.	n.d.	n.d.	100
4[d]	1.97	n.d.	n.d.	n.d.	100
5[e]	3.44	n.d.	n.d.	n.d.	100
6[f]	3.85	n.d.	n.d.	n.d.	100

[a] Reaction conditions: photocatalyst (entry is **MIL-125-RV^{2+}**), MeCN (25 mL), TEOA (5 mL), CO_2 (1 atm), λ = 420-800 nm (Visible light), 25 °C, 10 h. [b] Using Triisopropanolamine (TIPA) instead of TEOA. [c] Without TEOA. [d] Using H_2O (30 mL) as reaction medium. [e] Using H_2O (25 mL) and TIPA (5 mL) as reaction medium. [f] Using H_2O (25 mL) and TEOA (5 mL) as reaction medium.

Note: All measured using the same instruments, optical set-up except reaction conditions listed in the table. n.d. = Not detectable.

Table S5 Fitting analysis results of fluorescence lifetime of **MIL-125-NH_2 and MIL-125-RV^{2+}**.

Fluorescence lifetime (τ)	τ_1 (ns)	τ_2 (ns)	τ_3 (ns)
MIL-125-NH_2	0.711 (39.32 %)	3.303 (41.61 %)	17.349 (19.07%)
MIL-125-RV^{2+}	1.078 (40.59 %)	4.424 (41.49 %)	23.909 (17.92 %)

References

1. M. A. Syzgantseva, C. P. Ireland, F. M. Ebrahim, B. Smit and O. A. Syzgantseva, *J. Am. Chem. Soc.*, 2019, **141**, 6271-6278.
2. A. Leblanc, N. Mercier, M. Allain, M. C. Dul, G. Weber, N. Geoffroy, J. P. Bellat and I. Bezverkhyy, *Dalton Trans.*, 2017, **46**, 15666-15670.
3. D. Barbier, C. Marazano, C. Riche, B. C. Das and P. Potier, *J. Org. Chem.*, 1998, **63**, 1767-1772.
4. T. Gong, X. Yang, Q. Sui, Y. Qi, F.-G. Xi and E.-Q. Gao, *Inorg. Chem.*, 2016, **55**, 96-103.
5. S. Aduru, S. Contarini and J. W. Rabalais, *J. Phys. Chem.*, 1986, **90**, 1683-1688.
6. D. Dai, J. Qiu, L. Zhang, H. Ma and J. Yao, *J. Colloid Interface Sci.*, 2022, **607**, 933-941.
7. B. Zhang, J. Zhang, X. Tan, D. Shao, J. Shi, L. Zheng, J. Zhang, G. Yang and B. Han, *ACS Appl. Mater. Interfaces*, 2018, **10**, 16418-16423.
8. H. Assi, L. C. Pardo Pérez, G. Mouchaham, F. Ragon, M. Nasalevich, N. Guillou, C. Martineau, H. Chevreau, F. Kapteijn, J. Gascon, P. Fertey, E. Elkaim, C. Serre and T. Devic, *Inorg. Chem.*, 2016, **55**, 7192-7199.
9. X.-M. Cheng, X.-Y. Dao, S.-Q. Wang, J. Zhao and W.-Y. Sun, *ACS Catal.*, 2021, **11**, 650-658.
10. M. A. Nasalevich, M. G. Goesten, T. J. Savenije, F. Kapteijn and J. Gascon, *Chem. Commun.*, 2013, **49**, 10575-10577.
11. L. Liu, Q. Liu, R. Li, M.-S. Wang and G.-C. Guo, *J. Am. Chem. Soc.*, 2021, **143**, 2232-2238.
12. B. Ding, H. Gao, C. Wang and X. Ma, *Chem. Commun.*, 2021, **57**, 3154-3157.
13. Z. Mi, P. Yang, R. Wang, J. Unruangsri, W. Yang, C. Wang and J. Guo, *J. Am. Chem. Soc.*, 2019, **141**, 14433-14442.
14. N. R. Babij, E. O. McCusker, G. T. Whiteker, B. Canturk, N. Choy, L. C. Creemer, C. V. D. Amicis, N. M. Hewlett, P. L. Johnson, J. A. Knobelsdorf, F. Li, B. A. Lorsbach, B. M. Nugent, S. J. Ryan, M. R. Smith and Q. Yang, *Org. Process Res. Dev.*, 2016, **20**, 661-667.
15. X. Wang, G. Yang, G. Chai, M. S. Nasir, S. Wang, X. Zheng, C. Wang and W. Yan, *Int. J. Hydrogen Energy*, 2020, **45**, 30634-30646.
16. T. Wang, L. Chen, C. Chen, M. Huang, Y. Huang, S. Liu and B. Li, *ACS Nano*, 2022, **16**, 2306-2318.
17. K.-Q. Hu, P.-X. Qiu, L.-W. Zeng, S.-X. Hu, L. Mei, S.-W. An, Z.-W. Huang, X.-H. Kong, J.-H. Lan, J.-P. Yu, Z.-H. Zhang, Z.-F. Xu, J. K. Gibson, Z.-F. Chai, Y.-F. Bu and W.-Q. Shi, *Angew. Chem. Int. Ed.*, 2020, **59**, 20666-20671.